



The evolution on the microstructure and thermal expansion behavior of Al–50Si alloy with different P contents

Tao Jiang¹ · Shiju Li¹ · Chuang Yu¹ · Jinyu Fu¹ · Bowen Wei¹ · Liangliang Luo¹ · Guangming Xu¹

Received: 7 December 2018 / Accepted: 20 February 2019 / Published online: 4 March 2019
© Springer Science+Business Media, LLC, part of Springer Nature 2019

Abstract

In the previous work, the Al–50Si alloy with fine primary Si is prepared by a low-cost technology. In addition, the morphology of primary Si and the metamorphic mechanism as well as the thermal expansibility of alloy are also investigated in this work. The mean size of primary Si can obtain the min value of 33.82 μm when the content of modifier is 3%. The thermal expansibility of alloy decreases with the increasing of modifier. The influence of microstructure, solid solubility as well as porosity on the thermal expansibility are also studied in this research. Moreover, several theoretical models such as ROM model, Turner model, Kerner model and Schapery model are also used to predict the coefficient of thermal expansion (CTE) of alloy.

1 Introduction

The electronic packaging refers to the packaging for electronic devices and components as well as electronic systems and so on, which is used for protecting circuits and chips from external environment [1, 2]. According to the requirements of modern electronic packaging, the properties needed for electronic packaging materials mostly comprise [3, 4]: (1) high thermal conductivity; (2) low coefficient of thermal expansion (CTE); (3) relatively high mechanical strength; (4) good processability; (5) low density; etc.

There are many kinds of traditional electronic packaging materials, such as ceramic materials (Al_2O_3 , AlN and SiC), plastic encapsulation and metal-matrix encapsulation materials. Al_2O_3 is the maturest ceramic materials used for electronic packaging for its low thermal expansion coefficient and complete preparation technology. However, due to the low thermal conductivity of Al_2O_3 , the application of this material is also limited. AlN is a new type of high thermal conductivity ceramic but it is not suitable for commercial production due to its complicated preparation process and high cost.

The Al–Si alloys synthesize the excellent performances of Al matrix and Si phase, which has advantages of high thermal conductivity, low thermal expansion coefficient, low density, good processability and low cost [5]. Thus, the Al–Si alloy can satisfy the requirements of modern electronic packaging for thermophysical and technological properties. Nevertheless, when the contents of Si exceed 20%, the high-silicon aluminum alloy used for electronic packaging cannot be fabricated by conventional casting process due to the coarsening of primary Si [6].

In order to refine primary Si, some metamorphic measures are used to improve the morphology of primary Si. The typical refining methods of primary Si are mainly in three ways shown as follows. One is chemical modification [7], which affects nucleation and growth of primary Si by using modifier. The other is rapid solidification [8, 9], which refines primary Si by improving nucleation rate of primary Si and restraining the diffusion of Si atoms. Moreover, some mechanical treatments are also used to refine primary Si, such as ultrasonic vibration [10], overheating treatment [11] and so on. Chemical modification, especially for P modification, is the most widely used method in industry due to its simple operation and low cost.

The Al–50Si alloys with various P contents researched in this work are prepared by water-cooled copper mold. Using the new mold with high cooling rate and the modifier with good metamorphic effect, we intend to fabricate a type of high-silicon aluminum alloy used for electronic packaging at a low cost.

✉ Guangming Xu
xu_gm@epm.neu.edu.cn

¹ Key Laboratory of Electromagnetic Processing of Materials of Ministry of Education, Northeastern University, Shenyang 110819, China

2 Experiments

The Al–50Si alloy used in this article are produced by using water-cooled copper mold whose thickness is 25 mm. Commercial pure Al (99.7%) and commercial pure Si (98%) are used as raw materials for manufacturing Al–50Si alloys. The Cu–14P alloys are used as modifier to refine the morphology of primary Si. The Al–50Si alloys are melted in a medium-frequency induction furnace, heated to 1200 °C and held for 10 min before casting.

In order to research the transformation on the morphology of primary Si under different P contents and metamorphic mechanism, a scanning electron microscopy (SEM) equipped with X-ray energy dispersive spectroscopy (EDS) is used to detect the composition and morphology of phases. Some SEM samples are mechanically ground to 1 µm diamond paper and then etched in a 20% NaOH solution for 20–80 s with the temperature of 80 °C. In order to quantitative analysis the size and form factor of Si phase in the Al–50Si alloy under different P contents, an image analyzer software (Image Pro Plus, IPP) is applied. The formulas for counting the size and form factor are shown as follows [12]:

$$S = \sqrt{4A/\pi} \quad (1)$$

$$F = 4\pi A/C^2 \quad (2)$$

where S means the size of Si phase, F signifies the shape factor, A represents the area of Si phase, C is the perimeter of Si phase.

The thermal expansion coefficient detected in this work is linear expansion coefficient which is tested by using a dilatometer with the type of DIL805A/D. The formula used to calculate the coefficient of thermal expansion (CTE) is shown as follows [13]:

$$\alpha = \frac{1}{L_0} \frac{\Delta L}{\Delta T} \quad (3)$$

where α is CTE, L_0 is the original length of samples, ΔT means the variations in temperature, ΔL is the variations of length with temperature. The samples used for thermal expansion experiment are designed as $\Phi 4 \times 10$ mm. The testing temperature is in the range from 50 to 500 °C with the heating rate of 5 K/min.

3 Results and discussion

3.1 Microstructures

Figure 1 shows the evolution of microstructure under different P contents. As presented in figure, the primary Si in the un-metamorphic alloy shows coarse plate-like in shape with the mean size of 130.47 µm. The primary Si

distribute nonuniformly in the matrix and also connect to each other, which will divide the matrix into many parts. When the content of modifier is 1%, due to the metamorphism of AIP phase, some octahedral primary Si with fine size can be seen in the alloy and the mean size of primary Si also decreases. However, most primary Si are still plate-like with high aspect ratio, which can be attributed to the over-metamorphic phenomenon caused by the shortage of modifier contents. The morphology of primary Si improves and the mean size also decreases with the increasing of modifier contents. When the content of Cu–P is elevated to 3%, all large primary Si disappear and are replaced by fine octahedral primary Si. The mean size of primary Si and corresponding standard deviation severally reach their min values of 33.82 µm and 15.66 µm at this modifier content. The smaller the standard deviation is, the less difference between the grain size and mean size is. Thus, the size of primary Si will be more homogeneous. When the content of modifier exceeds 3%, the size of primary Si enhances with the increasing of modifier content. The mean size of primary Si increases to 34.66 µm when the content of Cu–P is 5%. The over-metamorphic phenomenon begins to appear in the alloy during that time. When the content of modifier is 7%, the short rod-like primary Si can be observed in the matrix, which can be attributed to the over-metamorphic phenomenon caused by the severe aggregation of AIP phase in Al–50Si alloy.

In order to investigate the metamorphic mechanism, the distribution of Al, Si and P elements are detected by using surface scan method. According to the previous researches [14], the P elements in the alloy are mainly in the form of AIP phase. As seen in Fig. 2, some clusters of P element can be seen slightly in point A, which can be attributed to the reaction of AIP with water during sample preparation process. The reaction is shown as follows [15]:



Table 1 shows the crystal characteristics of Si and AIP phases [16]. Both Si and AIP phases are cubic crystal structures. The difference between the two lattice constants as well as the difference of min interatomic distance between two atoms are 0.42% and 4.9%, respectively. According to the orientation relationship between coherent interfaces, the corresponding interfaces between the two phases have same orientation relationship if the interatomic distance difference between the interfaces of two phases is lower than 5%. Therefore, the AIP particles can be the basement for heterogeneous nucleation of primary Si [17, 18].

Moreover, according to the classical solidification theory [19], the energy used for homogeneous and heterogeneous nucleation are:

$$\Delta G_K = \frac{4\pi r_K^2 \sigma}{3} \quad (5)$$

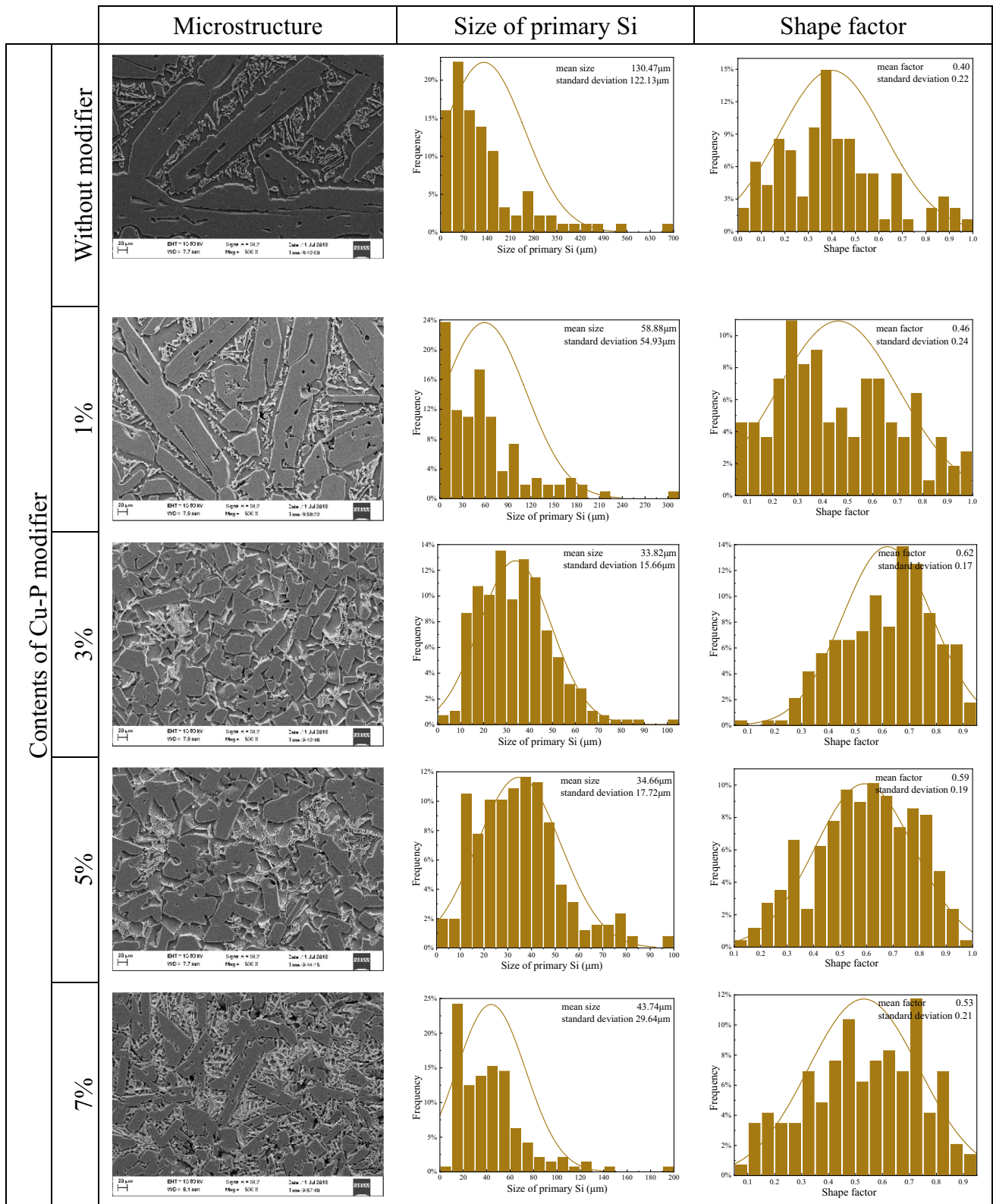


Fig. 1 The microstructures, sizes and shape factors of Al-50Si alloys with different modifier contents

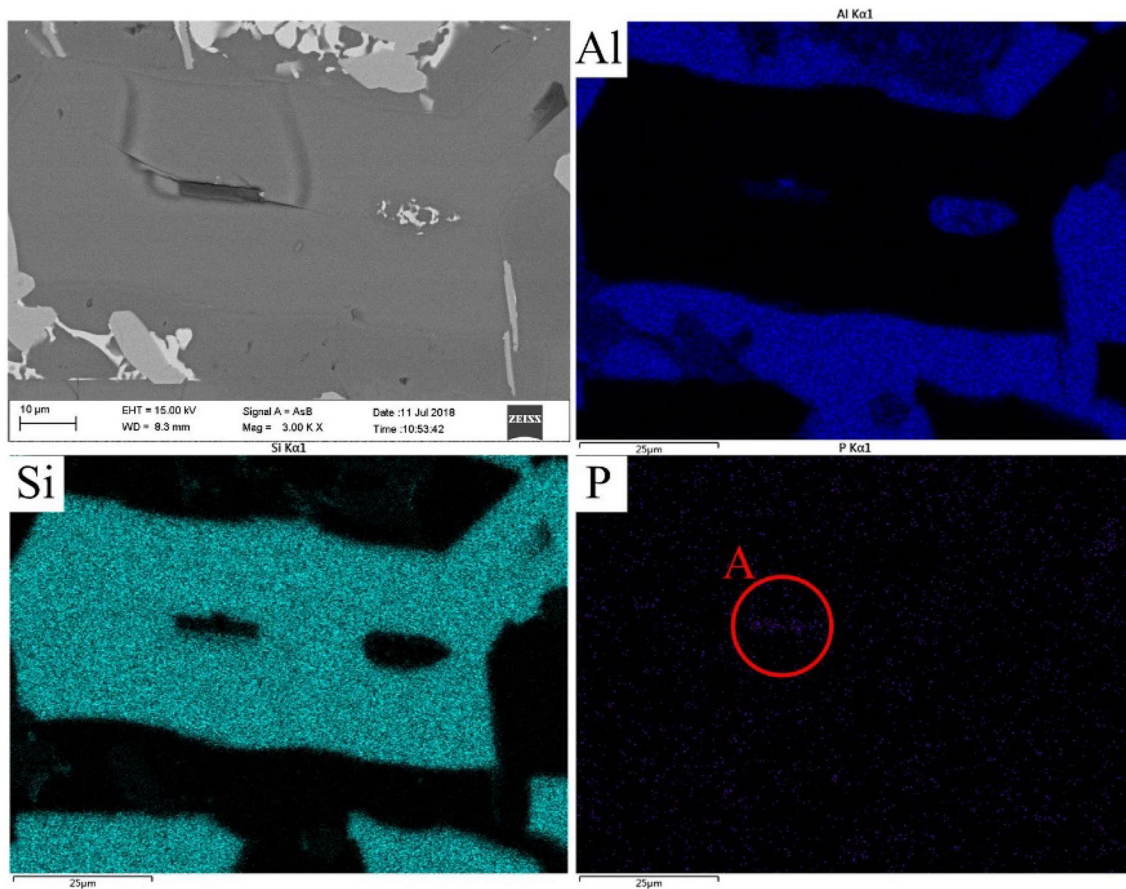


Fig. 2 EDX elements analysis of primary Si with 3% modifier content

Table 1 The crystal characteristic of Si and AlP

Crystal characteristic	Materials	
	Si	AlP
Crystal structure	Diamond-type	Zinc blende structure
Lattice constant (nm)	0.5428	0.5451
Min interatomic distance (nm)	0.244	0.256

and

$$\Delta G'_K = \frac{4\pi r_K'^2 \sigma}{3} \left(\frac{2 - 3 \cos \theta + \cos^3 \theta}{4} \right) \tag{6}$$

where ΔG_K and $\Delta G'_K$ are the energy of homogeneous and heterogeneous nucleation, respectively; r_K and r'_K mean the critical nucleus radius of homogeneous and heterogeneous nucleation; σ represents surface energy of unit area; θ is wetting angle.

It can be seen by taking the derivative of Formula 6 that the derivative of $\Delta G'_K$ is always greater than 0 when θ is between 0° and 180° , that is, the Formula 6 is an increasing function when θ is in the range of 0° – 180° . The $\Delta G'_K$ gets its max value of $4\pi r_K'^2 \sigma / 3$ when θ is 180° , which is equal to the result of ΔG_K . When θ is ranged from 0° to 180° , the energy used for heterogeneous nucleation is always lower than that for homogeneous nucleation. Thus, the Si atoms prefer to adhere to the dispersed AlP particles rather than combine with each other during solidification process so that the primary Si can be refined effectively.

Figure 3 shows the different morphologies of primary Si in Al–50Si alloys. The primary Si discussed in this article are mainly in the form of plate-like and octahedron-like in morphology. The morphology of primary Si changes from plate-like to octahedron-like with the increasing of P contents.

It can be seen from Fig. 3a that the primary Si in the un-metamorphic Al–50Si alloy shows plate-like with high aspect ratio. The plate-like primary Si in the hypereutectic Al–Si alloy has an external structure of facet feature with the outer surface of close-packed (111) plane [16]. The crystal

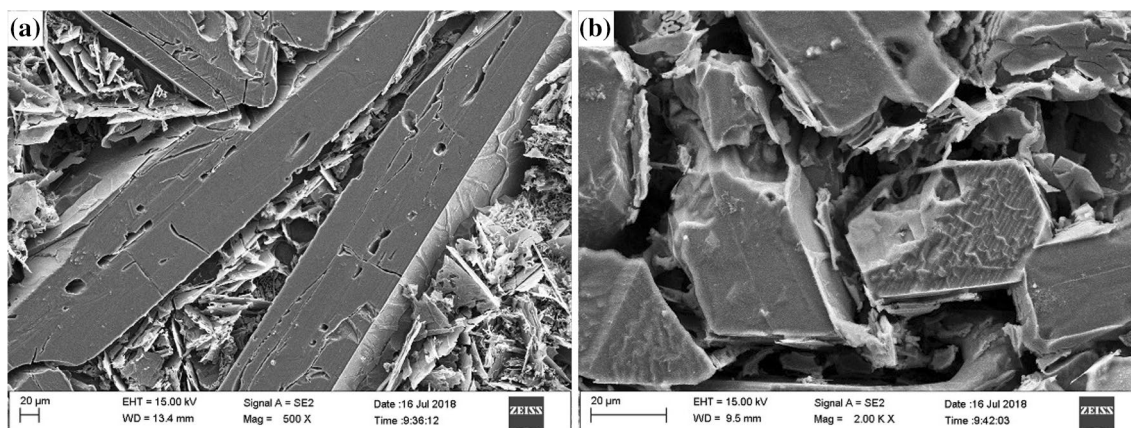


Fig. 3 The morphology of primary Si. **a** plate-like, **b** octahedron-like

atoms will be staggered arrangement and a number of twins will also form in the melt due to the undercooling and impurities existing at the front of solid–liquid interface during solidification process. The twins appearing at the growth front of primary Si create grooves and peaks whose angles are 141° and 219° , respectively [20]. Because the energy required to deposit atoms on the groove is lower than that on the smooth interface, the groove is a favorable position for atoms to aggregate and grow. Moreover, the atoms or clusters of Si deposited on the groove is easy to satisfy the condition of interfacial free energy for the growth of Si so that the Si phase grows rapidly at the groove and grow into plate-like eventually.

Some pores can also be seen near the central line of plate-like primary Si. Xu think that the appearing of holes can be attributed to the enrichment of impurity at the front of liquid–solid interface, which is relative to the growth mode of primary Si [21]. During the solidification process, a large number of impurities will enrich on the growth surface of Si phase with the growing of primary Si. The impurities enriched in the groove is difficult to diffuse comparing with that enriched at the edge of primary Si, which will make the concentration of impurities in groove higher than that at the edge. When the contents of impurities exceed a certain degree, the Si atoms in the groove will stop growing. However, the Si atoms will continue to accumulate at the edge of twins where the concentration of impurities is low, which will generate holes in grooves.

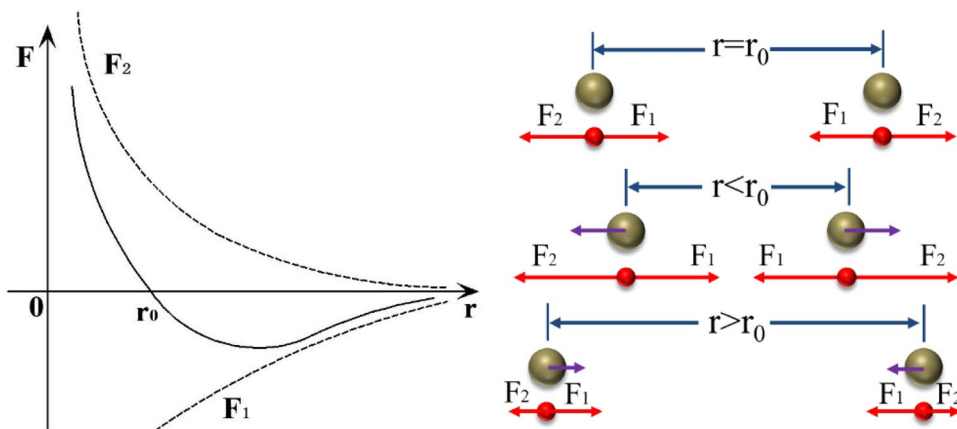
Figure 3b shows the morphology of polygonal primary Si. The octahedral primary Si in the alloy will be randomly cut at any angles during sample making process, which will leave some polygonal outlines on the specimen such as triangles and rectangles as well as hexagons and so on [22]. Therefore, the polygonal primary Si in the Al–50Si alloy should be the outline of cut octahedral primary Si. The holes in the center of the primary Si can be seen clearly in the

microstructure, which can be attributed to the corrosive effect of AIP phase. At the early stage of solidification, the Si atoms and clusters in the melt will prefer to absorb on AIP phase and form initial crystal nucleus due to the metamorphic effect of AIP. The Si crystal belongs to face-centered cubic (FCC) structure. The advantaged growth direction of face-centered cubic crystals is $[100]$ direction, i.e. $\langle 100 \rangle$, $\langle 010 \rangle$, $\langle 001 \rangle$, $\langle \bar{1}00 \rangle$, $\langle 0\bar{1}0 \rangle$ and $\langle 00\bar{1} \rangle$ directions [23]. The crystal nucleus will grow into a cross-shaped dendrite at first, which shows as three mutual perpendicular axes in space. The atoms existing at the end of dendrites accumulate along the edge of octahedron and form octahedral crystal nucleus skeleton [22]. With the growing of the cross-shaped dendrites, the Si atoms will connect with each other during the subsequent process and develop into octahedral crystal at last.

3.2 Thermal expansion behavior

Figure 4 shows the schematic diagram of the thermal expansion behavior. The nature of the thermal expansion behavior of solid materials can be attributed to the average distance (r) of particles in lattice increase with temperature. The interaction forces between adjacent particles are nonlinear during lattice vibration process, which means the force is not simply proportional to the displacement but exists an equilibrium position (r_0). The repulsive force increases rapidly with displacement when r is less than r_0 . But the attractive force increases slowly with displacement when r is greater than r_0 . The equilibrium position of particle vibration will shift to right side of r_0 under stress, which will increase the average distance of particles. The offset of equilibrium position and the average distance between adjacent particles increase with temperature, which will lead to the increasing of lattice

Fig. 4 The schematic diagram of the thermal expansion behavior. F_1 —attractive force; F_2 —repulsive force



parameters at the micro level and perform as thermal expansion behavior at the macro level.

Figure 5 shows the CTE of alloys under different P contents as a function of temperature. All curves in Fig. 5a show similar trend of variation, that is, the CTE increases at first and then decreases with the increasing of temperature. Moreover, at low temperature, the CTE of the modified alloys is lower than that of the un-metamorphic and owe-metamorphic alloys.

The Al matrix will do not have plastic deformation when the temperature is low. Thus, the CTE of the alloy will increase linearly with temperature due to the interaction of α -Al and primary Si in expansion. However, as the temperature continues to increase, the thermal stress on the interface between Al and Si phases will increase gradually and the yield strength will also continuously decrease. When the thermal stress exceeds yield strength of α -Al matrix, the alloy will generate plastic deformation. The thermal expansion of the Al–50Si alloy mainly comes from α -Al, but the expansion of Si as well as the plastic deformation of matrix will offset the partial

expansion of α -Al. The existing research results indicate that, with the increasing of temperature, the lattice of Al expands and the CTE increases [24]. Since the solid solubility of Si in Al increases with temperature, the lattice constant of Al will decrease, which will have negative effects on the thermal expansion of alloy.

The relationship between the lattice constant of Al and CTE can be described as [24]:

$$\alpha = \frac{1}{a_0} \frac{da}{dT} \tag{7}$$

where α represents CTE, a_0 is the inherent lattice constant of Al and da/dT means the variation of lattice constant with temperature. The a in formula 7 is a function of the solid solubility of Si in Al, which can be given by

$$a = a_0 + \frac{\Delta a}{\Delta C} C \tag{8}$$

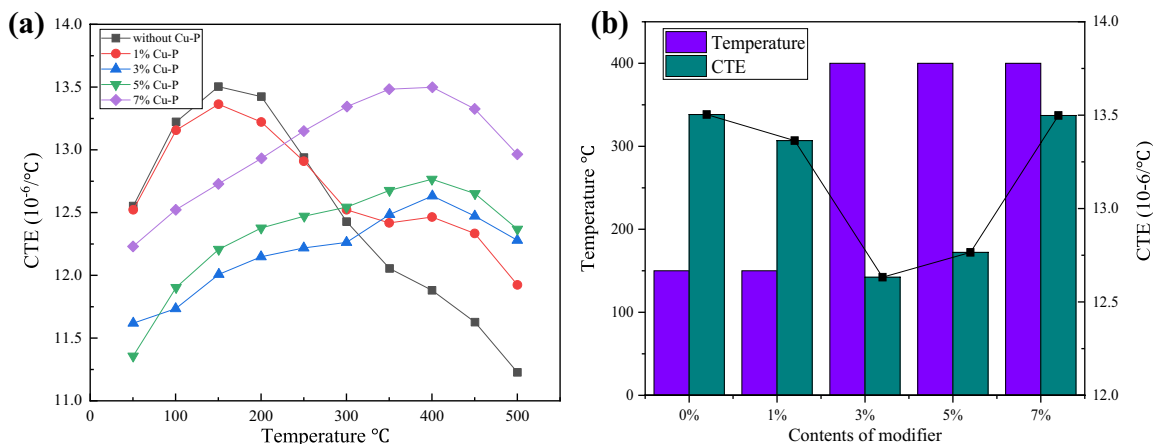


Fig. 5 The CTE curves of the Al–50Si alloy and the max values of CTE. **a** The CTE curves of the Al–50Si alloy; **b** The max values of CTE and the corresponding temperatures

where C is the solid solubility of Si in Al, which can be expressed by

$$C = Ae^{-\frac{\Delta H}{RT}} \quad (9)$$

where A is a constant, R is the universal gas constant and T is the Kelvin temperature. By combining the formulas mentioned above, the relationship between CTE and solid solubility can be described as

$$\alpha = \frac{1}{a_0} \frac{da_0}{dT} + \frac{1}{a_0} \frac{\Delta a}{\Delta C} Ae^{-\frac{\Delta H}{RT}} \frac{\Delta H}{RT^2} \quad (10)$$

The Al belongs to face-centered cubic structure with four atoms in a crystal cell. The lattice constant of Al is 0.4049 nm. Si belongs to diamond-type structure with eight atoms in a crystal cell. The lattice constant of Si is 0.5428 nm. The calculation results show that the average atomic volume of Al and Si are $1.65 \times 10^{-23} \text{ cm}^3$ and $2.01 \times 10^{-23} \text{ cm}^3$, respectively. The atomic volume of Si increases 21.8% by comparing with Al.

It can be seen from the formula 10 that the coefficient of thermal expansion of the alloy is mainly influenced by the solid solubility of Si in Al. With the increasing of temperature, plenty of Si atoms will dissolve into α -Al matrix. For the average atomic volume of Si mentioned above is bigger than that of Al atoms, the dissolution of Si in Al will decrease the lattice constant so that the CTE of alloy is also reduced. Moreover, due to the high temperature during melting process, the melt will absorb a large number of gases and generate many pores. During the heating process, the matrix will expand and fill in the pores, which will also be harmful to the expansion of alloy.

As seen in Fig. 5b that the peak value of CTE decreases at first and then increases with the increasing of P contents. The CTE of un-metamorphic and owe-metamorphic alloys reach their peak values of $13.50 \times 10^{-6} \text{ K}^{-1}$ and $13.36 \times 10^{-6} \text{ K}^{-1}$ when the temperature is 150 °C. When the content of modifier is 3%, the peak value of CTE reduces to $12.63 \times 10^{-6} \text{ K}^{-1}$ and the corresponding temperature is 400 °C. The CTE of alloy increases with P contents when the content of modifier exceeds 3%.

In consideration of the microstructure mentioned above, the primary Si in the un-metamorphic and owe-metamorphic Al–50Si alloys shows plate-like with high aspect ratio. With the increasing of P content, the morphology of primary Si changes from plate-like to fine and regular shape. The primary Si with fine and regular shape distributes homogeneously in the matrix, which will enhance the specific surface area of primary Si in the unit area and increase the interface between Si phase and α -Al [25]. In addition, Zhu et al. think that the expansion of Al–Si alloy is mainly influenced by the ductile α -Al phase [26]. Because the α -Al matrix does not form a whole connected grid with each other, the expansion of alloy is severely constraint. Thus, due to the enhancement

of restriction effect from Si to Al, the CTE of alloy reaches its min value and the temperature required to get the peak value of CTE also enhances when the content of modifier is 3%.

3.3 Theoretical models

Except for the content of each components, the CTE of alloy is also affected by many other factors. Somebody think that the CTE of alloy is influenced by the elastic matrix, the enhanceosome, the interaction between matrix and enhanceosome as well as the interfacial characteristics between them [27]. At present, the research on thermal expansion behavior shows that the theoretical models can be used to predict the CTE of Al–Si alloy after simplification. The rule of mixture of composite (ROM) is the most widely used and the simplest rule in analyzing the CTE of alloy. The ROM model can be expressed as [28]:

$$\alpha = \alpha_m V_m + \alpha_p V_p \quad (11)$$

where α is the coefficient of thermal expansion, V is the volume fraction of each component. Except for the ROM model, Turner model and Kerner model as well as Schapery model are also used to predict the CTE of Al–50Si alloy in this work. Turner model considers that the CTE of alloy is determined by matrix and enhanceosome. And it does not take the morphology and size of enhanceosome into account. The Turner model is defined [29]:

$$\alpha = \frac{\alpha_p V_p K_p + \alpha_m V_m K_m}{V_p K_p + V_m K_m} \quad (12)$$

where K is bulk modulus ($K = E/[3(1 - 2\mu)]$), μ represents Poisson ratio. Kerner model assumes the reinforcements as spherical particles and thinks that the distribution of matrix composition is homogeneously. According to the Kerner model [30], the CTE of Al–50Si alloy can be given by:

$$\alpha = \alpha_m V_m + \alpha_p V_p + V_p V_m (\alpha_p - \alpha_m) \times \frac{K_p - K_m}{V_m K_m + V_p K_p + \frac{3K_m K_p}{4G_m}} \quad (13)$$

where G is shear modulus ($G = E/[2(1 + \mu)]$). Schapery model also regards the reinforcements as spherical particles [31]. And it considers the interaction between each component. According to the Schapery model, the CTE of Al–50Si alloy can be calculated by:

$$\alpha_c = \alpha_p + (\alpha_m - \alpha_p) \times \frac{K_m (K_p - K_c)}{K_c (K_p - K_m)} \quad (14)$$

where K_c is given by the Hashin boundary condition. According to the previous researches, only upper and lower

boundary values can be calculated [32]. The upper and lower boundaries of K_c are shown as follows:

$$K_c^{upper} = K_p + \frac{V_m}{\frac{1}{K_m - K_p} + \frac{V_p}{K_p + \frac{4G_p}{3}}} \tag{15}$$

$$K_c^{lower} = K_m + \frac{V_p}{\frac{1}{K_p - K_m} + \frac{V_m}{K_m + \frac{4G_m}{3}}} \tag{16}$$

Some physical parameters used in the formulas mentioned above are presented in Table 2 [33].

Figure 6 shows the comparison between experimental results and theoretical values. As seen in figure that the CTE results calculated by four models show similar trend with the variation of temperature, that is, the calculated CTE results increase linearly with temperature. It can also be seen from figure that the theoretical results calculated by ROM are the highest among the four methods, the Turner results are the lowest. The calculation results of upper and lower boundary values of Schapery model is between the results of ROM and Turner model. The theoretical values of Kerner model is in line with the upper boundary values of Schapery model.

It can also be seen from figure that the experimental results in the curve without P content have large deviation with the four type of theoretical values, which can be attributed to the reason that all models neglect the influence of morphology and distribution of reinforcing phase on the CTE. Moreover, the effects of both solid solubility and porosity on the CTE are also not taken into account. It is worth noting that the actual values of curve with 3% Cu–P is in accord with the results predicted by lower boundary values of Schapery model and Kerner model when the temperature is between 100 and 300 °C. However, the experimental results are lower than the results predicted by four models when the temperature is higher than 300 °C. The difference between theoretical values and actual values under high temperature can be attributed to the reason that the Si phase will still play a restraining action on α -Al matrix due to the low expansibility of Si.

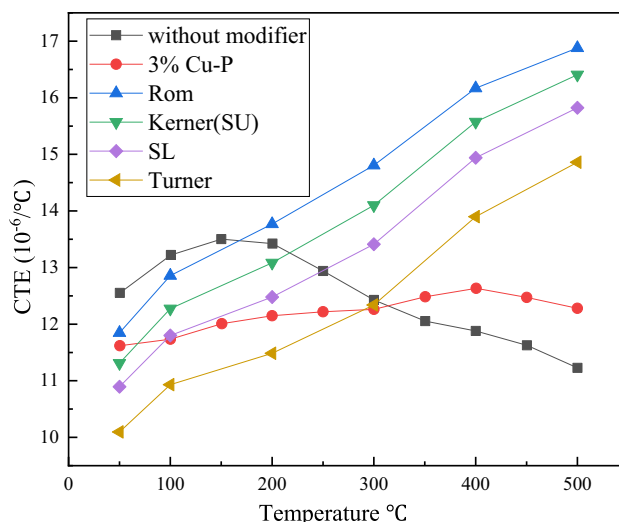


Fig. 6 The curves of experimental results and theoretical values

Moreover, the solid solubility and porosity also play an important role in the expansion of alloy. Thus, the deviation between theoretical values and actual values will generate under high temperature.

4 Conclusion

- (1) The addition of Cu–P modifier can effectively refine the morphology of primary Si. The min size of 33.82 μm can be achieved when the content of modifier is 3%.
- (2) The morphology of primary Si changes from plate-like to octahedron-like with the increasing of P contents.
- (3) The thermal expansibility of alloy is influenced by the morphology of primary Si and the solid solubility as well as porosity. The thermal expansibility is the lowest when the content of Cu–P is 3%.
- (4) The theoretical models can be used to predict the CTE of Al–50Si alloy with the modifier of 3% when the temperature is between 100 and 300 °C.

Table 2 Some physical parameters of Si and Al

Temperature/°C	Al				Si			
	E/GPa	G/GPa	K/GPa	CTE/(10 ⁻⁶ K ⁻¹)	E/GPa	G/GPa	K/GPa	CTE/(10 ⁻⁶ K ⁻¹)
50	69.2	26.0	67.8	22.6	163	66.8	97.0	2.5
100	67.6	25.4	66.3	24.2	162	66.4	96.4	3.0
200	64.0	24.1	62.7	25.7	161	66.0	95.8	3.4
300	59.8	22.3	62.3	27.7	160	65.6	95.2	3.6
400	54.9	20.2	65.4	30.4	156	63.9	92.9	3.8
500	49.9	18.1	69.3	31.7	157	64.3	93.4	4.0

References

1. X.C. Tong, *Advanced Materials for Thermal Management of Electronic Packaging*. (Springer, New York, 2011) pp. 39–65
2. L. Tian Minbo, Tongxiang, H. Wei. (1995) Electronic packaging technologies and materials. *Micronanoelectr. Technol.* **4**, 42–61
3. C. Zweben, Metal-matrix composites for electronic packaging. *JOM* **44**(7), 15–23 (1992)
4. C. Zweben, Advances in composite materials for thermal management in electronic packaging. *JOM* **50**(6), 47–51 (1998)
5. P.J. Ward, H.V. Atkinson et al., Semi-solid processing of novel MMCs based on hypereutectic aluminium-silicon alloys. *Acta Mater.* **44**(5), 1717–1727 (1996)
6. B. Heshmatpour, *Modification of Silicon in Eutectic and Hyper-Eutectic Al–Si Alloys. Essential Readings in Light Metals: Cast Shop for Aluminum Production*. (Wiley, New Jersey, 2013)
7. M. Zuo, X.F. Liu, Refinement of Hypereutectic Al–Si alloy by a new Al–Sc–P Master Alloy. *J. Inorg. Organomet. Polym Mater.* **22**(1), 64–69 (2012)
8. A. Leatham, Spray forming: alloys, products and markets. *Met. Powder Rep.* **54**(5), 28–37 (1999)
9. T.S. Kim, B.T. Lee, C.R. Lee, B.S. Chun, Microstructure of rapidly solidified Al–20Si alloy powders. *Materials Science and Engineering: A* **304**, 617–620 (2001)
10. C.H.E.N.G. He-fa et al., Influence of ultrasonic treatment on microstructure of hypereutectic Al–20%Si alloy. *Trans. Mater. Heat Treat.* **32**(3), 35–39 (2011)
11. LI, Yan-xia et al., Study on solidification behavior and microstructure of Al–25%Si alloy after melt superheating treatment. *China Foundry* **62**(4), 272–277 (2013)
12. Shu-sen, Wu et al., Development of non-dendritic microstructure of aluminum alloy in semi-solid state under ultrasonic vibration. *Solid State Phenom.* **141–143**, 451–456 (2008)
13. X. Zhu, R. Wang et al., Microstructure and thermal expansion behavior of spray-formed Al–27Si alloy used for electronic packaging. *J. Mater. Sci. Mater. Electr.* **25**(11), 4889–4895 (2014)
14. F. Cao et al., Evolution of microstructure and mechanical properties of as-cast Al–50Si alloy due to heat treatment and P modifier content. *Mater. Des.* **74**(7), 150–156 (2015)
15. Y. Jia et al., Microstructure and thermal conductivity of hypereutectic Al-high Si produced by casting and spray deposition. *J. Mater. Res.* **31**(19), 2948–2955 (2016)
16. H. Hui-fang., (2010) Study on the Si phase, Modification and Properties of Al–25%Si alloy. Doctoral dissertation, Chongqing University
17. R.Y. Wang et al., Growth morphology of primary silicon in cast Al–Si alloys and the mechanism of concentric growth. *J. Cryst. Growth* **207**(1), 43–54 (1999)
18. D. Li, M. Zuo et al., The investigation of continuous nucleation and refinement of primary Si in Al–30Si mushy zone. *J. Alloys Compd.* **502**(2), 304–309 (2010)
19. D.J. Fisher, *Fundamentals of Solidification*. (Trans Tech. Pub, New York, 1986)
20. X. Chen, Y. Zhong, T. Zheng, Z. Shen, J. Wang, L. Fan et al., Refinement of primary Si in the bulk solidified Al–20wt%Si alloy assisting by high static magnetic field and phosphorus addition. *J. Alloys Compd.* **714**, 39–46 (2017)
21. X. Chang-lin. (2007) Effect of modification on primary silicon in hypereutectic Al–Si alloys and modified mechanism. Doctoral dissertation, Jilin University
22. C.L. Xu, H.Y. Wang, C. Liu, Q.C. Jiang, Growth of octahedral primary silicon in cast hypereutectic Al–Si alloys. *J. Cryst. Growth* **291**(2), 540–547 (2006)
23. H.Q. Hu, *The Principle of Metal Solidification* (China Machine Press, Beijing, 1990)
24. T.A. Hahn, R.W. Armstrong, Internal stress and solid solubility effects on the thermal expansivity of Al–Si eutectic alloys. *Int. J. Thermophys.* **9**(2), 179–193 (1988)
25. C.W. Chien, S.L. Lee, J.C. Lin, M.T. Jahn, Effects of Si_p size and volume fraction on properties of Al/Si_p composites. *Materials Lett.* **52**(4), 334–341 (2002)
26. Z.H.U. Xuwei, W.A.N.G. Richu, P.E.N.G. Chaoqun, P.E.N.G. Jian, Microstructure and thermal expansion behavior of hypereutectic Al–Si alloy. *J. Central South Univ. (Science and Technology)* **47**(5), 1500–1505 (2016)
27. C.S. Park, C.H. Kim, M.H. Kim, C. Lee, The effect of particle size and volume fraction of the reinforced phases on the linear thermal expansion in the Al–Si–SiC_p system. *Mater. Chem. Phys.* **88**(1), 46–52 (2004)
28. T.W. Clyne, P.J. Withers, *An Introduction to Metal Matrix Composites* (Cambridge University press, New York, 1993)
29. N. Chawla, X. Deng, D.R.M. Schnell, Thermal expansion anisotropy in extruded SiC particle reinforced 2080 aluminum alloy matrix composites. *Mater. Sci. Eng. A* **426**(1), 314–322 (2006)
30. E.H. Kerner (1956) The elastic and thermo-elastic properties of composite media. *Proc. Phys. Soc. B* **69**(8), 808
31. R.A. Schapery, Thermal expansion coefficients of composite materials based on energy principles. *J. Compos. Mater.* **2**(3), 380–404 (1968)
32. Z. Hashin, S. Shtrikman, A variational approach to the elastic behavior of multiphase materials. *J. Mech. Phys. Solids* **11**, 127–140 (1963)
33. T. Huber, H.P. Degischer, G. Lefranc, T. Schmitt, Thermal expansion studies on aluminium-matrix composites with different reinforcement architecture of SiC particles. *Compos. Sci. Technol.* **66**(13), 2206–2217 (2006)

Publisher's Note Springer Nature remains neutral with regard to jurisdictional claims in published maps and institutional affiliations.